

Fig. 6. (A) Normalized ρ_c , and (B) M as a function of a H parallel to the c axis at various $T < T_{max}^c$ for a sample with demagnetizing factor $N/4\pi \approx 0.08$ of the $\text{La}_{2-x}\text{Sr}_{1+2x}\text{Mn}_2\text{O}_7$ ($x = 0.3$) crystal.

CPP-MR than current-in-plane (CIP)-MR in artificial magnetic multilayers (16). The merit of the perovskite manganites is that the spin polarization η of the conduction electrons is very large (reaching 100% at $T \ll T_c$) as compared with the case of conventional FM transition metal [for example, for Ni, $\eta \approx 11\%$ (17)]. Therefore, the interplane tunneling probability should be very sensitive to the respective spin states in the adjacent MnO_2 bilayers.

In the configuration with H parallel to the c axis ($H \parallel c$), the samples for Figs. 3 and 5 [$\sim 1 \times 1 \times 0.08$ (c axis) mm^3] have a large demagnetizing factor [$N/4\pi \approx 0.9$, which was estimated by using the correction for ellipsoids with three different axes (18)]. Thus, the real saturation field H_{sat} for this configuration should be much smaller than that presented in Fig. 5. To minimize the demagnetizing effect, we measured both the field dependence of the interplane MR and M for a sample with small demagnetizing factor for $H \parallel c$ [$1.04 \times 0.28 \times 1.88$ (c axis) mm^3 , $N/4\pi \approx 0.08$]. Figure 6 displays the results with $H \parallel c$ at several T 's below T_{max}^c . Below 40 K, the MR is rather insensitive to T . Small but clear hystereses were observed in isothermal MR curves, perhaps reflecting a high sensitivity of resistance measurement, though the hysteresis was not clearly discernible in the M curves. With increasing T toward T_{max}^c , the saturated resistivity further decreases because of the additional MR effect arising from the field alignment of the thermally fluctuated magnetic domain along the c axis.

The MR ratio $[\rho_c(0) - \rho_c(H_{sat})]/\rho_c(H_{sat})$ could vary from sample to sample, or from electrode to electrode, or both. In our measurements, the ratios were 30 up to 240% at temperatures sufficiently below T_{max}^c . Although the origin of the scatter in the data has not been understood yet, a statistical distribution of the interplane magnetic domain boundaries might be responsible. H_{sat} , which appears around 1 kOe in the sample for Fig. 6, will be ~ 400 Oe when the demagnetization effect is properly corrected.

We have presented the interplane tunneling MR in a layered manganite crystal, $\text{La}_{2-2x}\text{Sr}_{1+2x}\text{Mn}_2\text{O}_7$ ($x = 0.3$), which is viewed as composed of FM-metallic MnO_2 bilayers with intervening nonmagnetic insulating $(\text{La,Sr})_2\text{O}_2$ blocks. In the 2D FM region, T_{max}^c (~ 100 K) $\leq T \leq T_{max}^{ab}$ (~ 270 K), the field-induced incoherent-coherent transition for the interplane (c axis) charge transport contributes mostly to the extremely large MR effect. Even below the interplane spin-ordering temperature T_{max}^c , the interplane tunneling of the almost fully spin-polarized electrons is blocked at the interplane magnetic domain boundaries on the insulating $(\text{La,Sr})_2\text{O}_2$ layers, but is recovered during the magnetization process. This field-sensitive tunneling process gives rise to a low-field (< 1 kOe) MR as large as $\geq 200\%$. The layered manganite thus intrinsically contains the infinite arrays of FM/I/FM junctions in its crystal structure, and shows a colossal interplane tunneling MR.

REFERENCES AND NOTES

1. M. N. Baibich *et al.*, *Phys. Rev. Lett.* **61**, 2472 (1988).
2. S. S. P. Parkin, Z. G. Li, D. J. Smith, *Appl. Phys. Lett.* **58**, 2710 (1991).
3. A. E. Berkowitz *et al.*, *Phys. Rev. Lett.* **68**, 3745 (1992); J. Q. Xiao, J. S. Jiang, C. L. Chien, *ibid.*, p. 3749.
4. B. Dieny *et al.*, *Phys. Rev. B* **43**, 1297 (1991).
5. T. Miyazaki and N. Tezuka, *J. Magn. Magn. Mater.* **139**, L231 (1995).
6. For example, K. Chahara, T. Ohno, M. Kasai, Y. Kozono, *Appl. Phys. Lett.* **63**, 1990 (1993); S. Jin *et al.*, *Science* **264**, 413 (1994).
7. C. Zener, *Phys. Rev.* **82**, 403 (1951); P. W. Anderson and H. Hasegawa, *ibid.* **100**, 675 (1955); P.-G. de Gennes, *ibid.* **118**, 141 (1960); K. Kubo and N. Ohta, *J. Phys. Soc. Jpn.* **33**, 21 (1972).
8. H. Kuwahara *et al.*, *Science* **272**, 80 (1996).
9. M. Julliere, *Phys. Lett. A* **54**, 225 (1975); S. Maekawa and U. Gefvert, *IEEE Trans. Magn.* **18**, 707 (1982).
10. Y. Moritomo, A. Asamitsu, H. Kuwahara, Y. Tokura, *Nature* **380**, 141 (1996).
11. Y. Tomioka, A. Asamitsu, H. Kuwahara, Y. Moritomo, Y. Tokura, *Phys. Rev. B* **53**, R1689 (1996).
12. Y. Okimoto *et al.*, *Phys. Rev. Lett.* **75**, 109 (1995).
13. Y. Maeno *et al.*, *Nature* **372**, 532 (1994).
14. For example, S. L. Cooper and K. E. Gray, in *Physical Properties of High Temperature Superconductors IV*, D. M. Ginsberg, Ed. (World Scientific, Singapore, 1994), chap. 3.
15. T. G. Perring, G. Aeppli, Y. Moritomo, Y. Tokura, preprint.
16. M. A. M. Gijs, S. K. J. Lenczowski, J. B. Giesbers, *Phys. Rev. Lett.* **70**, 3343 (1993).
17. P. M. Tedrow and R. Meservey, *Phys. Rev. B* **7**, 318 (1973).
18. J. A. Osborn, *Phys. Rev.* **67**, 351 (1945).
19. We thank G. Aeppli, Y. Moritomo, R. Kumai, M. Kasai, and B. Raveau for helpful discussions. This work, supported in part by NEDO, was performed in JRCAT under the joint research agreement between NAIR and ATP.

16 August 1996; accepted 17 October 1996

Large-Scale Synthesis of Aligned Carbon Nanotubes

W. Z. Li, S. S. Xie,* L. X. Qian, B. H. Chang, B. S. Zou, W. Y. Zhou, R. A. Zhao, G. Wang

Large-scale synthesis of aligned carbon nanotubes was achieved by using a method based on chemical vapor deposition catalyzed by iron nanoparticles embedded in mesoporous silica. Scanning electron microscope images show that the nanotubes are approximately perpendicular to the surface of the silica and form an aligned array of isolated tubes with spacings between the tubes of about 100 nanometers. The tubes are up to about 50 micrometers long and well graphitized. The growth direction of the nanotubes may be controlled by the pores from which the nanotubes grow.

The discovery of carbon nanotubes (1) has led to much speculation about their properties and potential applications (2). Large quanti-

ties of carbon nanotubes can now be produced by either arc discharge (3, 4) or thermal deposition of hydrocarbons (5, 6). However, experimental characterizations and applications of the nanotubes have been hampered because of problems with the alignment of the nanotubes.

Recently, Ajayan *et al.* (7) developed a simple method to produce aligned arrays of carbon nanotubes by cutting a polymer resin-

W. Z. Li, S. S. Xie, B. H. Chang, B. S. Zou, W. Y. Zhou, R. A. Zhao, G. Wang, Institute of Physics, Chinese Academy of Sciences, Beijing 100080, China.
L. X. Qian, Department of Physics, Central University of Nationalities, Beijing 100081, China.

*To whom correspondence should be addressed. E-mail: user412@aphy01.iphys.ac.cn

nanotube composite. However, the degree of orientation of the nanotubes in the composite was affected by the thickness of the slices, and the aligning effect becomes less pronounced with increasing slice thickness. In addition, the presence of the resin matrix is unfavorable for accurately measuring the properties of the nanotubes. Another approach to aligning carbon nanotubes was reported by de Heer *et al.* (8), who produced a uniform black deposit by drawing a nanotube suspension through a 0.2- μm -pore ceramic filter and then transferring the deposited material onto a plastic surface to form a film of aligned carbon nanotubes. However, this results in some nanotubes sticking together, and the different lengths of the nanotubes in the film also affect the properties of the film. Recently, the synthesis of bundles of long, well-aligned single-walled nanotubes was reported (9).

We report here an efficient method to produce large areas of highly ordered, isolated long carbon nanotubes. The method is based on the chemical vapor deposition as described

previously (5, 6, 10, 11). However, instead of using carbon black (5) and graphite or silica covered with transition metal nanoparticles (6, 10, 11) as the substrate, we utilized mesoporous silica containing iron nanoparticles embedded in the pores.

Mesoporous silica containing iron nanoparticles were prepared by a sol-gel process from tetraethoxysilane (TEOS) hydrolysis in iron nitrate aqueous solution (12). Analytically pure TEOS (10 ml) was mixed with 10.4 ml of analytically pure ethyl alcohol and 0.1 M iron nitrate aqueous solution (11.4 ml) by magnetic stirring for ~ 30 min. A few drops of concentrated hydrogen fluoride (0.2 ml) were then added, and the mixture was stirred for 15 min. After gelation of the mixture, the gel was dried for 1 week at 60°C to remove the excess water and other solvents. The gel was then calcined 10 hours at 450°C at 10^{-2} torr. A silica network with relatively uniform pores was obtained with iron oxide nanoparticles embedded in the pores. The iron oxide nanoparticles were then reduced at 550°C in 180

torr of flowing 9% H_2/N_2 ($110\text{ cm}^3/\text{min}$) for 5 hours to obtain iron nanoparticles, which have a high catalytic activity. Subsequently, a mixture of 9% acetylene in nitrogen was introduced into the chamber at a flow rate of $110\text{ cm}^3/\text{min}$, and carbon nanotubes were formed on the substrate by deposition of carbon atoms obtained from decomposition of acetylene at 700°C (6, 10). The samples were examined by a scanning electron microscope (SEM) (S-4200, Hitachi) before and after carbon deposition, and energy-dispersive x-ray spectra (EDX) were recorded by a SiLi detector attached to the SEM. To prepare a transmission electron microscope (TEM) specimen, the sample was ground in a mortar and suspended in ethanol; a drop was then placed on a holey carbon copper grid and examined in a JEM 200-cx microscope to characterize the carbon nanotubes.

We have used this method to prepare films composed of large quantities of highly aligned carbon nanotubes (Fig. 1A). The films can be easily cleaved along the growth direction of the nanotubes, which demonstrates that individual nanotubes grow continuously from the bottom to the top of the films. The tip structure of the nanotubes (Fig. 1B) appears to be similar to that of β -aligned tubes reported in (8). The tube tips in the top view appear to be larger than the tube diameters in Fig. 2A in part because of an artifact caused by focusing and local charging effects and in part because of carbon clusters formed by the sudden stop of the growth process in our experiment.

At high magnification, the SEM image (Fig. 2A) shows that carbon nanotubes with diameters of ~ 30 nm grow out separately from the substrate to form an array; the spacing between the nanotubes is ~ 100 nm, which is consistent with the spacing between the pores on the substrate (Fig. 2B). Most of the carbon nanotubes are approximately perpendicular to the surface of the silica, although a few of the nanotubes are slightly curved or tilted. In order to verify the effect of the nanometer pores on the growth direction of the nanotubes, a quartz plate coated with the same iron nitrate solution, after drying and reduction, was used as the substrate to produce carbon nanotubes under the vapor deposition conditions described above. Many carbon nanotubes 30 nm in diameter were formed on the quartz plate, but these tubes grew randomly to form a thick layer. We speculate that the growth direction and distribution of the nanotubes are affected by the iron nanoparticles embedded in the pores of the mesoporous substrate, the pores acting as growth templates for carbon nanotubes.

High-magnification TEM images show that the carbon nanotubes are well graphitized and typically consist of ~ 40 concentric shells of carbon sheets (Fig. 3). Only a small

Fig. 1. (A) Low-magnification SEM image of a film composed of aligned carbon nanotubes. This film with a thickness of $\sim 50\ \mu\text{m}$ was obtained by growing for 2 hours. (B) Tip structure of the aligned tubes.

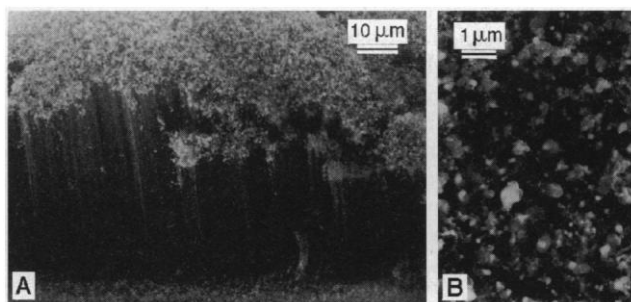


Fig. 2. (A) High-magnification SEM image of carbon nanotubes growing out from the mesoporous iron/silica substrate and forming an array. These carbon nanotubes have diameters of ~ 30 nm. Spacings between tubes are ~ 100 nm. Most of the carbon nanotubes are approximately perpendicular to the surface of the silica. (B) SEM image of the mesoporous iron/silica substrate before carbon deposition. Pores ~ 30 nm in diameter are distributed on the substrate and are separated by ~ 100 nm. Many pores have relatively regular circular openings, while others have irregular openings.

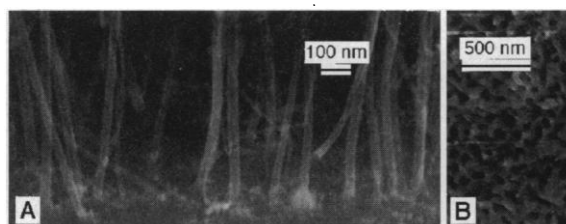


Fig. 3. High-resolution TEM image of a carbon nanotube. The tube is well graphitized and consists of about 40 concentric shells of carbon sheets with spacing between the sheets of 0.34 nm. The inner and outer diameters of the tube are 4 and 34 nm, respectively. Several TEM specimens have been examined carefully, but no carbon nanoparticles or iron nanoparticles trapped inside the tubes were observed, indicating that the carbon nanotube arrays are very pure.



amount of carbonaceous material is at the periphery of the carbon nanotubes. We have not found any filled tubes (13) or carbon nanoparticles (buckyonions) (14). We also varied the preparation conditions of the iron/silica substrate and found that the pore sizes were affected by the process parameters, such as stoichiometric composition, temperature, and drying procedure. The diameters of the carbon nanotubes were correspondingly affected. By applying the same conditions, it is easy to reproduce a specific substrate and obtain carbon nanotubes of the same diameter. The smallest diameter of carbon nanotubes prepared by our method to date is ~ 10 nm. We believe that it is possible to produce arrays consisting of very thin, and possibly even single-layered (4) carbon nanotubes, by improving the growth conditions.

EDX spectra taken from the tips of aligned tubes show that the tips are composed mainly of carbon and a small amount of iron (98.76 and 1.09 weight %, respectively). Some areas of the tube tips contain trace amounts of silicon and oxygen, both less than 0.2 weight %, which may be attributed to small silica fragments. The iron peak is attributed to iron nanoparticles which might have been pushed up by the growing carbon nanotubes. EDX spectra taken from central parts of the tubes show only a carbon peak; tubes filled with iron particles in the central parts were not detected. The TEM and EDX results indicate that some of the iron nanoparticles were attached firmly to the silica network and did not move upward during the growth of the carbon nanotubes, whereas others were attached weakly and could be carried up by the growing nanotubes.

In order to describe the formation mechanism of the array of aligned carbon nanotubes, a possible growth model is depicted in Fig. 4. With careful preparation, iron/silica substrates with uniform pores can be obtained (see also

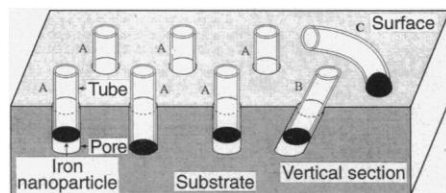


Fig. 4. Possible growth model of carbon nanotubes formed on iron nanoparticles embedded in mesoporous silica. Carbon nanotubes formed on iron nanoparticles embedded in the vertical cylindrical pores grow perpendicular to the surface of the substrate (marked A). Those formed on iron nanoparticles embedded in inclined cylindrical pores were tilted along the axes of the pores (marked B), whereas those formed on iron nanoparticles exposed on the surface of the substrate might grow freely (marked C). Tip or base growth is determined by the contact force between the iron nanoparticles and the silica network.

Fig. 2B). Most of the cylindrical pores are formed perpendicular to the surface of the substrate, and only very few of the cylindrical pores are inclined with respect to the surface of the substrate, as shown on the vertical section of the substrate in Fig. 4. We propose that the carbon nanotubes grow out from iron nanoparticles embedded in these pores and that the template effect of the pores constrains the carbon nanotubes to grow along the axis of the pores. Nanotubes formed on some exposed iron nanoparticles on the surface of the substrate may grow freely. Several models have been postulated to explain the formation mechanism of carbon nanotubes prepared by the catalytic decomposition of organic vapors (13, 15, 16). It is generally accepted that the tubes grow by the extrusion of carbon, dissolved in a metallic catalyst particle that is oversaturated in carbon at one part of the surface, and that the catalyst particles promote tip growth or base growth depending on the contact force between the catalyst particles and the substrate (16). In the present case, tip and base growth probably both occur; the tubes may be growing out from iron nanoparticles fixed in the pores, or the catalyst particles may be driving growth at the tube tips (13, 16). How the catalyst particles trapped in the pores affect the growth process is still an open question and needs further study. However, no matter which growth process takes effect, the growth directions will be constrained by the pores, resulting in aligned growth of the carbon nanotubes.

Recently, the synthesis of nanotubes inside the pores of a nanoporous alumina membrane through polymerization of acrylonitrile has been reported (17). However, the tubes did not grow out and had to be further graphitized at higher temperature. In contrast, carbon nanotubes produced by our method are relatively long and well graphitized, and the array of carbon nanotubes formed on the hard bulk-substrate can be easily manipulated for measuring its properties and applications. The length of the nanotubes increased with the growth time, the growth rate being about $25 \mu\text{m}/\text{hour}$. If the growth time was too long, some amorphous carbon was deposited on the surface of the carbon nanotubes, and with increasing length, the carbon nanotubes curved slightly. Optimal growth times were 2 to 5 hours, leading to lengths of the carbon nanotubes between 50 and $100 \mu\text{m}$.

In order to obtain large areas of aligned carbon nanotubes, mesoporous iron/silica substrates with large flat surfaces and uniform distribution of pores are required. A main obstacle of preparing large area mesoporous iron/silica substrates is that these materials tend to shrink, crack, and shatter during the preparation, so a meticulous dry-

ing procedure for the gelled iron/silica network has to be followed (12). By using large area mesoporous iron/silica substrates, we have successfully produced arrays of well-aligned and isolated carbon nanotubes of several square millimeters. The substrate has been successfully removed to retain aligned tubes. EDX spectra taken from the root of the nanotubes demonstrate the presence of carbon alone, neither silicon nor iron could be detected. This is evidence of firm attachment to the silica network of those iron nanoparticles that remain in the pores during nanotube growth.

Recent work has shown that carbon nanotubes show promise as a field emission source (18) and that they possess special electrical transport properties (8, 19) and high stiffness (20). We believe that the approach outlined here is a step toward the production of aligned nanotubes over large areas, and that our aligned, isolated, and long carbon nanotubes will offer more opportunities for both fundamental research and technological applications.

REFERENCES AND NOTES

1. S. Iijima, *Nature* **354**, 56 (1991).
2. J. W. Mintmire, B. I. Dunlap, C. T. White, *Phys. Rev. Lett.* **68**, 631 (1992); N. Hamada, S. Sawada, A. Oshiyama, *ibid.*, p. 1579; D. H. Robertson, D. W. Brenner, J. W. Mintmire, *Phys. Rev. B* **45**, 12592 (1991); M. S. Dresselhaus, *Nature* **358**, 195 (1992); R. Saito, M. Fujita, G. Dresselhaus, M. S. Dresselhaus, *Appl. Phys. Lett.* **60**, 2204 (1992).
3. T. W. Ebbesen and P. M. Ajayan, *Nature* **358**, 220 (1992); D. T. Colbert *et al.*, *Science* **266**, 1218 (1994).
4. D. S. Bethune *et al.*, *Nature* **363**, 605 (1993).
5. M. Endo *et al.*, *J. Phys. Chem. Solids* **54**, 1841 (1993).
6. V. Ivanov *et al.*, *Chem. Phys. Lett.* **223**, 329 (1994).
7. P. M. Ajayan, O. Stephan, C. Colliex, D. Trauth, *Science* **265**, 1212 (1994).
8. W. A. de Heer *et al.*, *ibid.* **268**, 845 (1995).
9. A. Thess *et al.*, *ibid.* **273**, 483 (1996).
10. M. J. Yacamán, M. M. Yoshida, L. Rendón, J. G. Santiesteban, *Appl. Phys. Lett.* **62**, 657 (1993).
11. H. Dai, E. W. Wong, Y. Z. Lu, S. Fan, C. M. Lieber, *Nature* **375**, 769 (1995); E. W. Wong, B. W. Maynor, L. D. Burns, C. M. Lieber, *Chem. Mater.* **8**, 2041 (1996); C. E. Snyder *et al.*, International Patent WO 89/07163 (1989).
12. B. M. Novak, *Adv. Mater.* **5**, 422 (1993).
13. S. Amelinckx *et al.*, *Science* **265**, 635 (1994).
14. Y. Saito, T. Yoshikawa, M. Inagaki, M. Tomita, T. Hayashi, *Chem. Phys. Lett.* **204**, 277 (1993); S. Iijima, *J. Cryst. Growth* **50**, 675 (1980); V. P. Dravid *et al.*, *Science* **259**, 1601 (1993); D. Ugarte, *Chem. Phys. Lett.* **209**, 99 (1993); S. Seraphin, D. Zhou, J. Jiao, J. C. Withers, R. Loutfy, *Appl. Phys. Lett.* **63**, 2073 (1993).
15. X. F. Zhang *et al.*, *J. Cryst. Growth* **130**, 368 (1993).
16. R. T. K. Baker, *Carbon* **27**, 315 (1989).
17. R. V. Parthasarathy, K. L. N. Phani, C. R. Martin, *Adv. Mater.* **7**, 896 (1995).
18. W. A. de Heer, A. Châtelain, D. Ugarte, *Science* **270**, 1179 (1995); A. G. Rinzier *et al.*, *ibid.* **269**, 1550 (1995).
19. H. Dai, E. W. Wong, C. M. Lieber, *ibid.* **272**, 523 (1996); T. W. Ebbesen *et al.*, *Nature* **382**, 54 (1996).
20. M. M. J. Treacy, T. W. Ebbesen, J. M. Gibson, *Nature* **381**, 678 (1996).
21. We thank W. Liu, Y. Zhang, and C. Y. Wang for their assistance in TEM and SEM work. Supported in part by the National Natural Science Foundation of China.

1 August 1996; accepted 30 October 1996